

Communication

Pd-Decorated ZnO Hexagonal Microdiscs for NH₃ Sensor

Yi Li, Boyu Zhang, Juan Li, Zaihua Duan ^{*}, Yajie Yang, Zhen Yuan, Yadong Jiang and Huiling Tai

State Key Laboratory of Electronic Thin Films and Integrated Devices, School of Optoelectronic Science and Engineering, University of Electronic Science and Technology of China (UESTC), Chengdu 611731, China

* Correspondence: zaihuaduan@uestc.edu.cn

Abstract: The NH₃ sensor is of great significance in preventing NH₃ leakage and ensuring life safety. In this work, the Pd-decorated ZnO hexagonal microdiscs are synthesized using hydrothermal and annealing processes, and the gas sensor is fabricated based on Pd-decorated ZnO hexagonal microdiscs. The gas-sensing test results show that the Pd-ZnO gas sensor has a good response to NH₃ gas. Specifically, it has a good linear response within 0.5–50 ppm NH₃ at the optimal operating temperature of 230 °C. In addition, the Pd-ZnO gas sensor exhibits good repeatability, short response time (23.2 s) and good humidity resistance (10–90% relative humidity). This work provides a useful reference for developing an NH₃ sensor.

Keywords: gas sensor; NH₃ detection; ZnO hexagonal microdiscs; Pd-decorated ZnO

1. Introduction

NH₃ has important application in industry, but as a toxic gas, its leakage can pollute the environment and even endanger life and health [1–3]. In addition, NH₃ is also present in the exhaled breath of kidney disease patients. By detecting the exhaled NH₃, it is possible to achieve an early diagnosis of kidney disease [4–6]. Therefore, the NH₃ sensor has received widespread attention and rapid development in recent years.

Gas-sensing materials are crucial for gas sensors. For widely reported semiconductor NH₃ sensors, the NH₃ gas-sensing materials mainly include polyaniline (PANI) and its composites [1,7–9], oxides (ZnO, SnO₂, and TiO₂) and their composites [10–16], and other composite materials. Among them, the PANI-based gas sensors have good selectivity for NH₃ and can operate at room temperature, but their response/recovery speed and stability are insufficient [1,3,5–9]. Until now, the oxides and their composites are still the mainstream gas-sensing materials in the field of semiconductor NH₃ sensors due to their fast response/recovery speed and good stability [10–16]. Among various oxide gas-sensing materials, n-type ZnO with a wide bandgap (3.37 eV) and good thermal/chemical stability and its composites have been frequently used for developing semiconductor NH₃ sensors [10–12,17–33]. The NH₃ sensing performances of the bare ZnO are usually poor [10–12]. Firstly, by selecting different materials and constructing ZnO composites, it is a conventional strategy to improve the NH₃-sensing performance of ZnO-based NH₃ sensors, such as poly(3-hexylthiophene)/ZnO [17], polymethyl methacrylate/reduced graphene oxide (rGO)/ZnO [19], carbon/ZnO [20,27], poly-o-methoxyaniline/ZnO [21], rGO/ZnO [23], CuO/ZnO [25], CuPc/ZnO [26], rGO/ZnO/Si [28], and WO₃·H₂O/ZnO [29]. Secondly, the element doping and precious metal decoration are effective strategies to improve the NH₃ sensing performances of the bare ZnO, such as Cd-doped ZnO [18], Cr-doped ZnO [22], Cu and La co-doped ZnO [24], Mn-doped ZnO [30], Pt-ZnO [31], Ag-ZnO [32], and Au-ZnO [33]. In addition, the morphology structure of gas-sensing materials is also closely related to their gas-sensing performance [34–37]. ZnO has rich morphology structures, such as nanoparticles [10,19,20,22–25,27–32], nanorods [11,17,18,21,23,26,33], and nanoflakes [12], which have been widely used for fabricating NH₃ gas sensors. Among var-



Citation: Li, Y.; Zhang, B.; Li, J.; Duan, Z.; Yang, Y.; Yuan, Z.; Jiang, Y.; Tai, H. Pd-Decorated ZnO Hexagonal Microdiscs for NH₃ Sensor. *Chemosensors* **2024**, *12*, 43. <https://doi.org/10.3390/chemosensors12030043>

Academic Editor: Michele Penza

Received: 16 February 2024

Revised: 1 March 2024

Accepted: 5 March 2024

Published: 5 March 2024



Copyright: © 2024 by the authors. Licensee MDPI, Basel, Switzerland. This article is an open access article distributed under the terms and conditions of the Creative Commons Attribution (CC BY) license (<https://creativecommons.org/licenses/by/4.0/>).

ious methods for preparing micro- and nanomaterials, the hydrothermal method is a simple and high-yield method widely used in the preparation of gas-sensing materials [38,39].

Based on the above analysis, this work aims to fabricate an efficient NH_3 sensor based on ZnO. Specifically, we synthesized ZnO hexagonal microdiscs using a mild hydrothermal method at 80°C . In order to further improve the NH_3 -sensing performances of ZnO hexagonal microdiscs, the Pd-decorated ZnO (Pd-ZnO) hexagonal microdiscs were synthesized by combining annealing processes. The NH_3 -sensing performances of the ZnO and Pd-ZnO sensors were tested at different working temperatures and NH_3 concentrations. The results show that the Pd-ZnO sensor has a good linear response within a wide range of NH_3 (0.5–50 ppm) and exhibits a good humidity resistance at the optimal operating temperature of 230°C .

2. Materials and Methods

2.1. Synthesis and Characterizations of ZnO and Pd-ZnO Hexagonal Microdiscs

Zinc acetate dihydrate (ZnCH_3COO) $_2 \cdot 2\text{H}_2\text{O}$, $\geq 99.0\%$) and palladium chloride (PdCl_2 , $\geq 99.0\%$ metals basis) were purchased from Shanghai Aladdin Chemical Reagent Co., Ltd. (Shanghai, China). Ammonia solution (AR, 25%) was purchased from Chengdu Jinshan Chemical Reagent Co., Ltd. (Chengdu, China).

Figure 1a shows the schematic diagram of the preparation process of ZnO and Pd-ZnO hexagonal microdiscs. Firstly, 1.756 g ZnCH_3COO) $_2 \cdot 2\text{H}_2\text{O}$ was added to 40 mL deionized water and vigorously stirred for 5 min to form 0.2 mol/L zinc acetate suspension. Secondly, the diluted ammonia solution was slowly added to zinc acetate suspension and stirred until the pH was about 9.5. Thirdly, the above zinc acetate suspension was transferred to a polytetrafluoroethylene lined stainless steel autoclave and heated to 80°C for 20 h. Finally, the ZnO hexagonal microdiscs were obtained by washing with ethanol and deionized water several times and centrifugation, which was followed by drying in an oven at 60°C . In order to obtain ZnO hexagonal microdiscs with a Pd decoration ratio of 0.1 wt%, 8.3 mg PdCl_2 and 0.5 g of the above-synthesized ZnO hexagonal microdiscs were dissolved in ethanol solution (1 mL) and thoroughly mixed. The mixture was dried in air at 80°C and annealed at 350°C for 1 h to finally obtain Pd-ZnO hexagonal microdiscs.

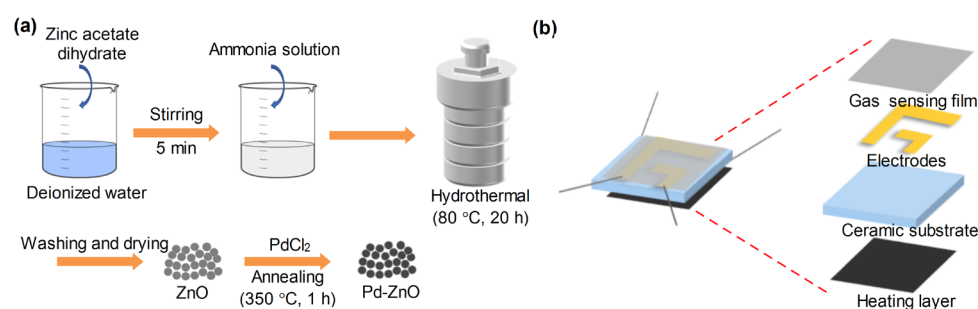


Figure 1. (a) Schematic diagram of the preparation process of ZnO and Pd-ZnO hexagonal microdiscs. (b) Schematic diagram of sensor structure.

ZnO and Pd-ZnO hexagonal microdiscs were characterized using field emission scanning electron microscopy (SEM, FEI Inspect F, Hillsboro, USA), X-ray diffractometer (XRD, Empyrean, PANalytical, Netherlands; $\lambda = 0.15406$ nm) and X-ray photoelectron spectroscopy (XPS, Thermo Scientific, Waltham, USA).

2.2. Fabrication and Gas-Sensing Performances Testing of Sensors

The ZnO and Pd-ZnO gas sensors were fabricated by a brush-coating method, and the detailed process can refer to our previous works [40,41]. The schematic diagram of the sensor structure is shown in Figure 1b, which is mainly composed of a heating layer, ceramic substrate, electrodes, and gas-sensing film. In short, the ZnO and Pd-ZnO hexagonal microdiscs were ground into pastes using deionized water and mortar. Then, the

ZnO and Pd-ZnO pastes were evenly brushed onto the Al₂O₃ ceramic substrates (length, width, and height: 1.5 mm, 1.5 mm, 0.25 mm) with a pair of Au interdigitated electrodes (electrodes width and distance: 0.3 mm). Finally, the ZnO and Pd-ZnO gas sensors were obtained by drying at 60 °C for 1 h. According to our previous test result [40], the thickness of the gas-sensing film is approximately 40 μm.

The gas-sensing evaluations of ZnO and Pd-ZnO gas sensors were completed through a homemade dynamic gas-sensing measurement system, which can be found in detail in our previous works [40–43]. Different gas concentrations (0.5–50 ppm NH₃) and relative humidity (RH) were controlled by three mass flow controllers (NH₃ (or selective gas) pipeline, humidity gas pipeline, dry air pipeline), and the resistance value of the sensor was recorded by a digital multimeter (Keithley 2700). According to the response characteristics of n-type ZnO and Pd-ZnO gas sensors to reducing gases, the response of the sensor is defined as R_a/R_g (R_a and R_g are the resistances of the gas sensors in air and target gas, respectively) [44,45]. The response and recovery times are defined as the time required for a 90% change in resistance of the sensor during adsorption and desorption processes [44–46]. Except for the humidity influence test (10–90% RH), all other tests were conducted at 50% RH.

3. Results and Discussion

3.1. Characterization

Figure 2 shows the SEM images of ZnO and Pd-ZnO. The ZnO is formed by stacking hexagonal microdiscs, which is attributed to the suppression of growth along the C-axis ([0001]) [47–49]. The diameter of hexagonal microdiscs is about 2 μm. Similarly, the Pd-ZnO is also formed by stacking hexagonal microdiscs, and due to the introduction of Pd and the annealing process, some micro- and nanoparticles are scattered on the surface of hexagonal microdiscs.

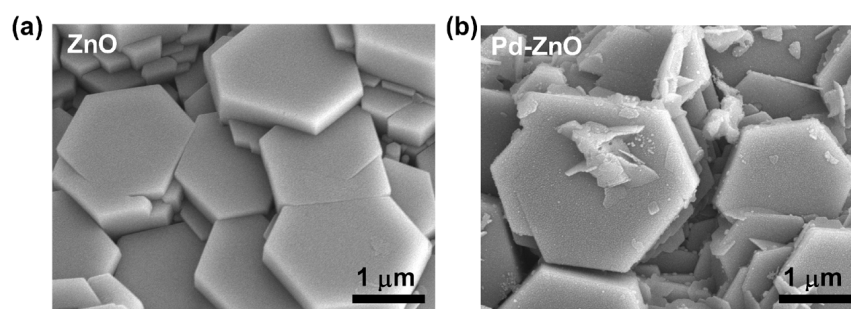


Figure 2. SEM images of (a) ZnO and (b) Pd-ZnO hexagonal microdiscs.

Figure 3a shows the XRD patterns of ZnO and Pd-ZnO. All diffraction peaks match well with the standard JCPDS card of ZnO (No. 36-1451), indicating that the synthesized ZnO can be attributed to the wurtzite ZnO with hexagonal structure [50–52]. It should be noted that there is no significant difference in the diffraction peaks between Pd-ZnO and ZnO, as the content of Pd is very low (0.1 wt%) and difficult to detect by XRD [53]. To confirm the elemental compositions of the materials, Figure 3b shows XPS full spectrums of ZnO and Pd-ZnO, revealing the expected Zn and O elements. In addition, the Pd element can also be seen in the Pd-ZnO spectrum (~340 eV), confirming its existence.

The O 1s spectrums of ZnO and Pd-ZnO are shown in Figure 3c,d, which can be divided into the chemisorbed oxygen species (O_C), oxygen vacancy (O_V) and lattice oxygen (O_L), respectively [13,15,21,42,45,54]. Compared to ZnO, the oxygen vacancy content in Pd-ZnO is higher, which may be attributed to the strong oxygen-binding capacity of Pd [43]. Oxygen vacancies are beneficial for adsorbing gas molecules, so the Pd-ZnO gas sensor with higher oxygen vacancy content is expected to achieve a better gas-sensing response [13,15,21,42,45,54].

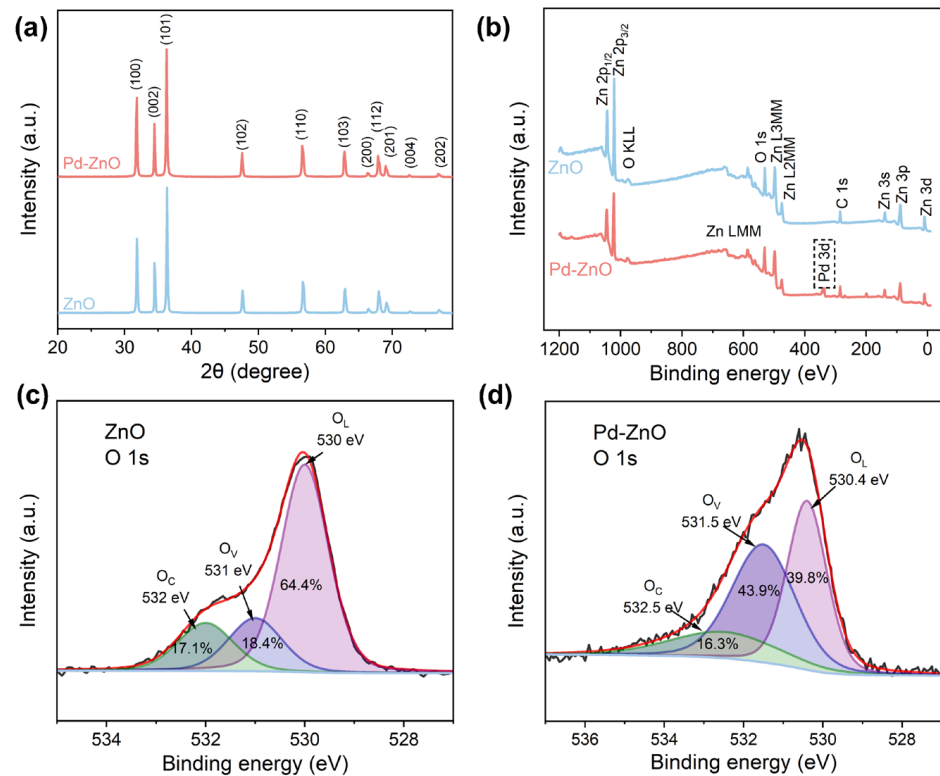


Figure 3. (a) XRD patterns of ZnO and Pd-ZnO. (b) XPS full spectrums of ZnO and Pd-ZnO. O 1s spectrums of (c) ZnO and (d) Pd-ZnO.

3.2. Gas-Sensing Performances

For oxide semiconductor gas sensors, their response is usually affected by the operating temperature [31,42,44,45]. Figure 4a shows the response values of ZnO and Pd-ZnO sensors toward 50 ppm NH₃ under different working temperatures. As the working temperature increases, the response values of ZnO and Pd-ZnO sensors first increase and then gradually decrease, exhibiting a typical “volcanic” response characteristic [31,42,44,45]. Overall, the response of the Pd-ZnO sensor is greater than that of the ZnO sensor. At 230 °C, the Pd-ZnO sensor has a maximum response of 3.9. Therefore, the working temperature for subsequent testing of the Pd-ZnO sensor is fixed at 230 °C. Figure 4b shows the resistive response and recovery curves of the Pd-ZnO sensor for 0.5–50 ppm NH₃, demonstrating its good response and recovery characteristics. Based on the response resistance values at different NH₃ concentrations in Figure 4b, the response results can be obtained as shown in Figure 4c. According to the linear fitting line, the Pd-ZnO sensor has a good linear response in a wide range NH₃ (0.5–50 ppm). Figure 4d shows that the Pd-ZnO sensor has a good repetitive response at 50 ppm NH₃. Through an amplified response and recovery curve in Figure 4e, the response and recovery times of the Pd-ZnO sensor are about 23.2 s and 271.8 s at 50 ppm NH₃. As shown in Table 1 [55–60], the proposed Pd-ZnO NH₃ sensor has competitive performances in response value, detection range and response speed compared to some of the reported oxide-based NH₃ sensors at heating operation. In addition, the response value and low concentration detection of the Pd-ZnO sensor also have certain advantages compared to some commercial oxide-based NH₃ sensors (MQ137 (Winsen), TGS26 (Figaro), TGS2444 (Figaro) and TGS824 (Figaro)).

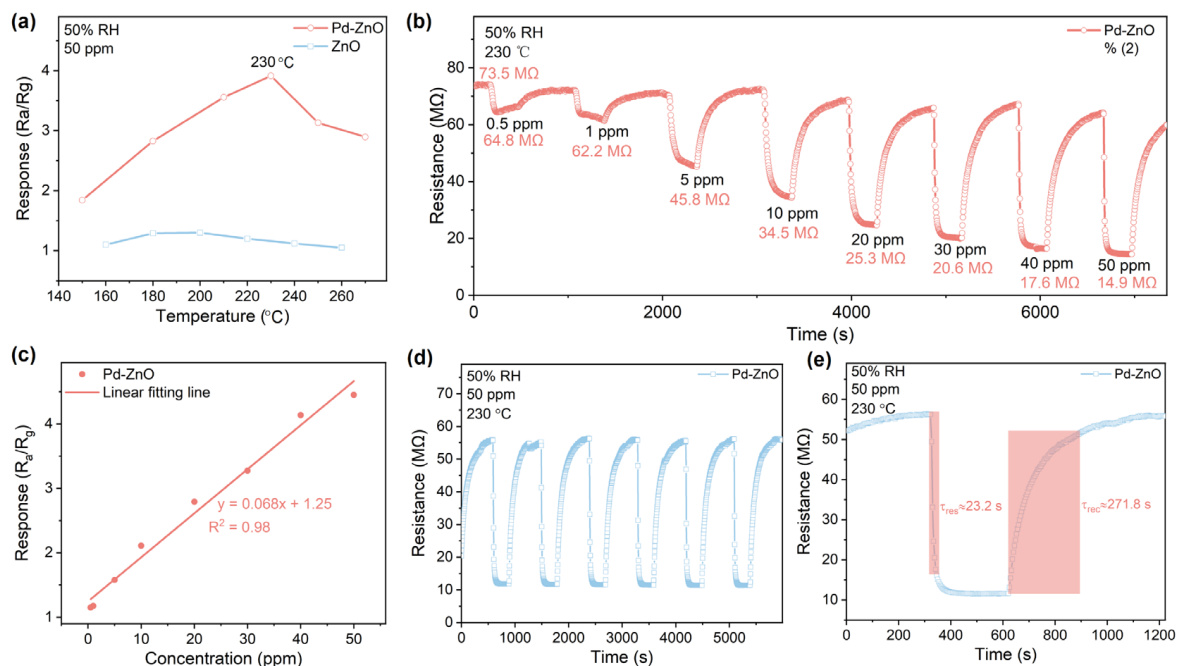


Figure 4. (a) Gas response values of ZnO and Pd-ZnO sensors toward 50 ppm NH₃ at different working temperatures. (b) Resistive response and recovery curves of Pd-ZnO sensor for 0.5–50 ppm NH₃. (c) Linear fitting line of response and NH₃ concentration. (d) Repetitive response and recovery curve at 50 ppm NH₃. (e) Response and recovery times at 50 ppm NH₃.

Table 1. Comparisons of the proposed Pd-ZnO NH₃ sensor with the reports and commercial NH₃ sensors.

Materials	Working Temperature (°C)	Response (Resistance Ratio)	Detection Range (ppm)	Response Time (s)	Refs.
ZnO nanoparticles	150	~1.57 (600 ppm)	50–600	160	[55]
TiO ₂ nanospheres	250	~2 (300 ppm)	100–400	5	[56]
Pd-TiO ₂ nanoparticles	500	~1.8 (400 ppm)	-	150	[57]
WO ₃ nanoparticles	400	4 (50 ppm)	25–100	-	[58]
SnO ₂ nanowires	400	~1.6 (40 ppm)	10–40	>120	[59]
Mo-SnO ₂ nanoparticles	350	3.1 (50 ppm)	20–100	21	[60]
SnO ₂	-	~2 (50 ppm)	5–500	~8	MQ137 (Winsen)
SnO ₂	-	~0.55 (150/50 ppm)	30–300	-	TGS826 (Figaro)
SnO ₂	-	~0.84 (100/30 ppm)	10–100	-	TGS2444 (Figaro)
SnO ₂	-	~0.5 (150/50 ppm)	30–300	-	TGS824 (Figaro)
Pd-ZnO hexagonal microdiscs	230	3.9 (50 ppm)	0.5–50	23.2	This work

Although the comfortable environment humidity is about 50% RH, the humidity in the environment is variable. For this reason, the resistive response and recovery curves of the Pd-ZnO gas sensor for 50 ppm NH₃ were tested under different RHs, as shown in Figure 5a. Under low humidity (10% and 30% RH), the recovery speed of the sensor is slow and incomplete. To observe changes of baseline and response resistance values, Figure 5b shows the base and response resistance curves of the Pd-ZnO gas sensor. As the RH increases, the baseline resistance of the sensor decreases due to the adsorption of water molecules [42]. More intuitively, Figure 5c shows the response and recovery curves from resistive response and recovery curves in Figure 5a. Correspondingly, the response

values of 50 ppm NH_3 under different RHs are shown in Figure 5d. Overall, within a wide humidity range of 10–90% RH, although the response of the Pd-ZnO gas sensor decreases due to the competitive adsorption of water molecules, the change is not significant, and it exhibits a good humidity resistance. Figure 6 shows that the Pd-ZnO gas sensor has certain selectivity and long-term stability. Selectivity is a major challenge faced by metal oxide semiconductor gas sensors, including ZnO, and we need to continuously seek solutions.

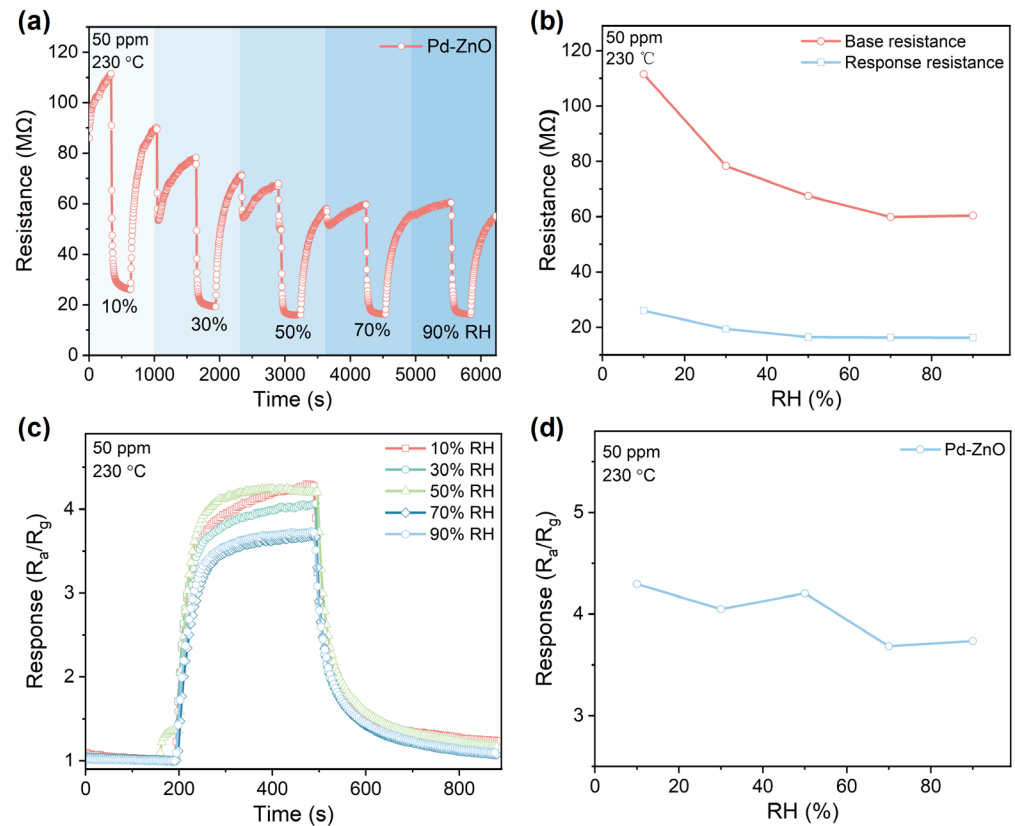


Figure 5. (a) Resistive response and recovery curves, (b) base and response resistance curves, (c) response and recovery curves, and (d) response values for 50 ppm NH_3 under different RHs.

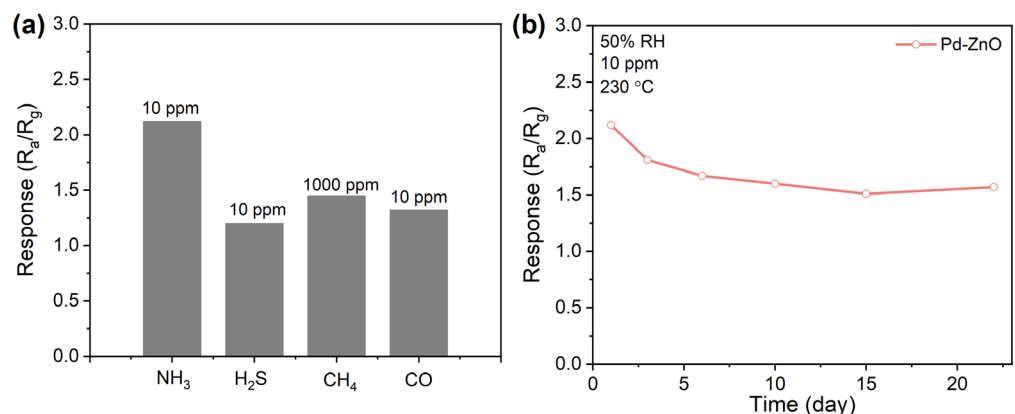


Figure 6. (a) Selective response for different gases. (b) Long-term stability for three weeks.

3.3. Gas-Sensing Mechanism

As a typical n-type gas-sensing material, the gas-sensing mechanism of ZnO has been widely discussed. Combining with Pd decoration, the enhanced NH_3 response mechanism of the Pd-ZnO gas sensor is discussed as follows. Firstly, according to the working temperature of 230 °C, the main type of adsorbed oxygen is O^- (100–300 °C) [61].

As shown in Figure 7a, when the Pd-ZnO gas sensor is exposed to air, the oxygen will adsorb on the surface of ZnO to form adsorbed oxygen ($O_2 + 2e^- \rightarrow 2O^-$), resulting in the electrons consumption and resistance increase in the Pd-ZnO gas sensor. When the Pd-ZnO gas sensor is exposed to NH_3 gas, the NH_3 gas will adsorb on the surface of ZnO and release electrons ($2NH_3 + 7O^- \rightarrow 3H_2O + 2NO_2 + 7e^-$), resulting in an increase in electrons and a decrease in sensor resistance, forming NH_3 sensing response (Figure 7b) [12]. Secondly, the introduction of Pd forms more oxygen vacancies in ZnO, which helps to adsorb NH_3 . In addition, the catalytic effect of Pd is conducive to the NH_3 oxidation and electrons release. Therefore, the Pd-ZnO gas sensor has a better NH_3 sensing response than the ZnO gas sensor [31–33].

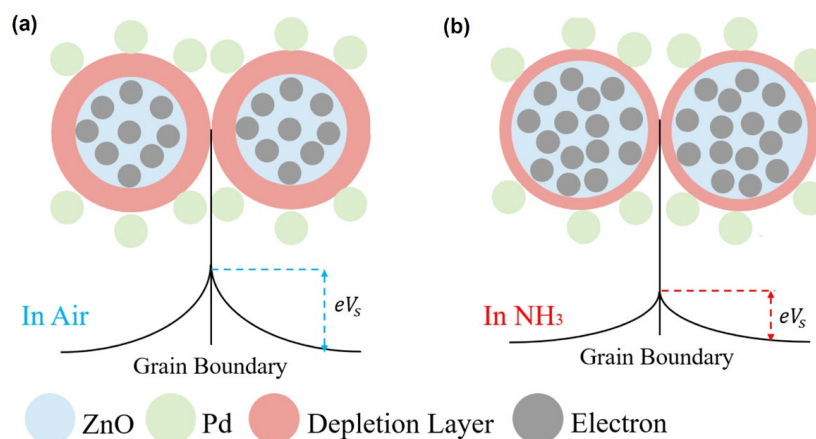


Figure 7. Schematic diagrams of the space charge layer changes of Pd-ZnO gas sensor. (a) In air and (b) In NH_3 .

4. Conclusions

In summary, we synthesized ZnO hexagonal microdiscs using a simple hydrothermal method and investigated its NH_3 sensing performances. In order to improve the NH_3 sensing response of bare ZnO hexagonal microdiscs, the Pd-decorated ZnO hexagonal microdiscs were prepared by combining mechanical mixing and annealing processes. The results show that the Pd-ZnO sensor has a larger NH_3 sensing response than that of the bare ZnO sensor at an optimal working temperature of 230 °C. The Pd-ZnO sensor exhibits a wide detecting range (0.5–50 ppm NH_3), good repeatability, short response time (23.2 s) and good humidity resistance. The enhanced NH_3 sensing response is explained by the catalytic effect of Pd. This work provides useful guidance for developing an NH_3 sensor.

Author Contributions: Conceptualization, B.Z., J.L. and Z.D.; methodology, B.Z. and J.L.; validation, Y.L., B.Z. and J.L.; formal analysis, B.Z., J.L., Z.Y. and H.T.; investigation, B.Z. and J.L.; data curation, Y.L., B.Z., Y.Y. and Y.J.; writing—original draft preparation, Y.L.; writing—review and editing, Z.D., Y.Y., Z.Y., Y.J. and H.T.; supervision, Y.Y.; project administration, Y.J. and H.T.; funding acquisition, Z.D. and Z.Y. All authors have read and agreed to the published version of the manuscript.

Funding: This work is supported by the Natural Science Foundation of China (Grant No. 62301114 and 62101105).

Institutional Review Board Statement: Not applicable.

Informed Consent Statement: Not applicable.

Data Availability Statement: The data of our study are available upon request.

Conflicts of Interest: The authors declare no conflicts of interest.

References

1. Kumar, V.; Mirzaei, A.; Bonyani, M.; Kim, K.H.; Kim, H.W.; Kim, S.S. Advances in electrospun nanofiber fabrication for polyaniline (PANI)-based chemoresistive sensors for gaseous ammonia. *TrAC Trends Anal. Chem.* **2020**, *129*, 115938. [[CrossRef](#)]
2. Bannov, A.G.; Popov, M.V.; Brester, A.E.; Kurmashov, P.B. Recent advances in ammonia gas sensors based on carbon nanomaterials. *Micromachines* **2021**, *12*, 186. [[CrossRef](#)]
3. Tang, X.; Debliquy, M.; Lahem, D.; Yan, Y.; Raskin, J.P. A review on functionalized graphene sensors for detection of ammonia. *Sensors* **2021**, *21*, 1443. [[CrossRef](#)]
4. Shetty, S.S.; Jayarama, A.; Bhat, S.; Satyanarayan; Karunasagar, I.; Pinto, R. A review on metal-oxide based trace ammonia sensor for detection of renal disease by exhaled breath analysis. *Mater. Today Proc.* **2022**, *55*, 113–117. [[CrossRef](#)]
5. Li, H.Y.; Lee, C.S.; Kim, D.H.; Lee, J.H. Flexible room-temperature NH₃ sensor for ultrasensitive, selective, and humidity-independent gas detection. *ACS Appl. Mater. Interfaces* **2018**, *10*, 27858–27867. [[CrossRef](#)]
6. Guntner, A.T.; Wied, M.; Pineau, N.J.; Pratsinis, S.E. Rapid and selective NH₃ sensing by porous CuBr. *Adv. Sci.* **2020**, *7*, 1903390. [[CrossRef](#)]
7. Li, J.; Dong, S.; Duan, Y.; Fu, X.; Li, G.; Huang, Y. Polyaniline composited with rGO wrapped-SiO₂ microsphere ammonia sensor with fast response/recovery and high sensitivity for pig healthy breeding. *Sens. Actuators B Chem.* **2024**, *398*, 134784. [[CrossRef](#)]
8. Hadano, F.S.; Gavim, A.E.X.; Stefanelo, J.C.; Gusso, S.L.; Macedo, A.G.; Rodrigues, P.C.; Mohd Yusoff, A.R.B.; Schneider, F.K.; Deus, J.F.; Jose da Silva, W. NH₃ sensor based on rGO-PANI composite with improved sensitivity. *Sensors* **2021**, *21*, 4947. [[CrossRef](#)]
9. Tanguy, N.R.; Thompson, M.; Yan, N. A review on advances in application of polyaniline for ammonia detection. *Sens. Actuators B Chem.* **2018**, *257*, 1044–1064. [[CrossRef](#)]
10. Al-darwesh, M.Y.; Ibrahim, S.S.; Faiad Naief, M.; Mishaal Mohammed, A.; Chebbi, H. Synthesis and characterizations of zinc oxide nanoparticles and its ability to detect O₂ and NH₃ gases. *Results Chem.* **2023**, *6*, 101064. [[CrossRef](#)]
11. Waikar, M.R.; Raste, P.M.; Sonker, R.K.; Gupta, V.; Tomar, M.; Shirsat, M.D.; Sonkawade, R.G. Enhancement in NH₃ sensing performance of ZnO thin-film via gamma-irradiation. *J. Alloys Compd.* **2020**, *830*, 154641. [[CrossRef](#)]
12. Kanaparthi, S.; Govind Singh, S. Highly sensitive and ultra-fast responsive ammonia gas sensor based on 2D ZnO nanoflakes. *Mater. Sci. Energy Technol.* **2020**, *3*, 91–96. [[CrossRef](#)]
13. Yuan, Y.; Zhan, G.; Peng, W.; Huang, C.; Chen, H.; Lin, S. Trace ppb-level NH₃ sensor based on single petal-like Ce-doped SnO₂. *Mater. Sci. Semicond. Process.* **2023**, *157*, 107335. [[CrossRef](#)]
14. Jiang, X.; Zhen, Y.; Feng, Y.; Yang, Z.; Qin, Z. Synthesis of SnS₂/SnO₂ nano-heterojunctions with increased reactive sites and charge transfer for ultrasensitive NH₃ detection. *J. Alloys Compd.* **2023**, *938*, 168520. [[CrossRef](#)]
15. Wu, K.; Debliquy, M.; Zhang, C. Room temperature gas sensors based on Ce doped TiO₂ nanocrystals for highly sensitive NH₃ detection. *Chem. Eng. J.* **2022**, *444*, 136449. [[CrossRef](#)]
16. Fernández-Ramos, M.D.; Capitán-Vallvey, L.F.; Pastrana-Martínez, L.M.; Morales-Torres, S.; Maldonado-Hódar, F.J. Chemoresistive NH₃ gas sensor at room temperature based on the carbon gel-TiO₂ nanocomposites. *Sens. Actuators B Chem.* **2022**, *368*, 132103. [[CrossRef](#)]
17. Han, K.X.; Wu, C.C.; Hsu, W.F.; Chien, W.; Yang, C.F. Preparation of ultrafast ammonia sensor based on cross-linked ZnO nanorods coated with poly(3-hexylthiophene). *Synth. Met.* **2023**, *299*, 117449. [[CrossRef](#)]
18. Brahma, S.; Huang, P.C.; Mwakikunga, B.W.; Saasa, V.; Akande, A.A.; Huang, J.L.; Liu, C.P. Cd doped ZnO nanorods for efficient room temperature NH₃ sensing. *Mater. Chem. Phys.* **2023**, *294*, 127053. [[CrossRef](#)]
19. Raza, A.; Abid, R.; Murtaza, I.; Fan, T. Room temperature NH₃ gas sensor based on PMMA/RGO/ZnO nanocomposite films fabricated by in-situ solution polymerization. *Ceram. Int.* **2023**, *49*, 27050–27059. [[CrossRef](#)]
20. Espid, E.; Lo, A.Y.; Taghipour, F. High performance UV-LED activated gas sensors based on ordered carbon mesoporous materials loaded with ZnO nanoparticles. *Mater. Sci. Eng. B* **2023**, *288*, 116203. [[CrossRef](#)]
21. Gao, R.; Ma, X.; Liu, L.; Gao, S.; Zhang, X.; Xu, Y.; Cheng, X.; Zhao, H.; Huo, L. In-situ deposition of POMA/ZnO nanorods array film by vapor phase polymerization for detection of trace ammonia in human exhaled breath at room temperature. *Anal. Chim. Acta* **2022**, *1199*, 339563. [[CrossRef](#)]
22. Nakarungsee, P.; Srirattanapibul, S.; Issro, C.; Tang, I.M.; Thongmee, S. High performance Cr doped ZnO by UV for NH₃ gas sensor. *Sens. Actuators A Phys.* **2020**, *314*, 112230. [[CrossRef](#)]
23. Gupta, S.; Ravikant, C.; Kaur, A. One-pot wet chemical synthesis of reduced graphene oxide-zinc oxide nanocomposites for fast and selective ammonia sensing at room temperature. *Sens. Actuators A Phys.* **2021**, *331*, 112965. [[CrossRef](#)]
24. Alagarasan, D.; Hegde, S.S.; Naik, R.; Murahari, P.; Shetty, H.D.; Prasad Hb, S.; Maiz, F.; Shkir, M. Fabrication of high-performance RT-NH₃ gas sensor based on Cu and La co-doped ZnO films through a facile drop-casting method. *Opt. Mater.* **2024**, *147*, 114705. [[CrossRef](#)]
25. Cheng, C.; Chen, C.; Zhang, H.; Zhang, Y. Preparation and study of ammonia gas sensor based on ZnO/CuO heterojunction with high performance at room temperature. *Mater. Sci. Semicond. Process.* **2022**, *146*, 106700. [[CrossRef](#)]
26. Huang, J.; Jiang, D.; Zhou, J.; Ye, J.; Sun, Y.; Li, X.; Geng, Y.; Wang, J.; Du, Y.; Qian, Z. Visible light-activated room temperature NH₃ sensor base on CuPc-loaded ZnO nanorods. *Sens. Actuators B Chem.* **2021**, *327*, 128911. [[CrossRef](#)]
27. Fan, S.X.; Tang, W. Synthesis, characterization and mechanism of electrospun carbon nanofibers decorated with ZnO nanoparticles for flexible ammonia gas sensors at room temperature. *Sens. Actuators B Chem.* **2022**, *362*, 131789. [[CrossRef](#)]

28. Yogi, S.; Kumar, A.; Kumar, P.; Kumar, V.; Zulfequar, M.; Jain, V.K. Trace level sensitivity and selectivity of room temperature NH₃ gas sensors based on RGO/ZnO@SiNWs heterostructure. *Phys. E* **2024**, *157*, 115864. [[CrossRef](#)]
29. Zhang, L.; Zhang, H.; Chen, C.; Hu, Z.; Wang, J. Preparation and mechanism of high-performance ammonia sensor based on tungsten oxide and zinc oxide composite at room temperature. *Curr. Appl. Phys.* **2023**, *45*, 30–36. [[CrossRef](#)]
30. Ramesh, A.; Gavaskar, D.S.; Nagaraju, P.; Duvvuri, S.; Vanjari, S.R.K.; Subrahmanyam, C. Mn-doped ZnO microspheres prepared by solution combustion synthesis for room temperature NH₃ sensing. *Appl. Surf. Sci. Adv.* **2022**, *12*, 100349. [[CrossRef](#)]
31. Li, Z.; Yi, J. Drastically enhanced ammonia sensing of Pt/ZnO ordered porous ultra-thin films. *Sens. Actuators B Chem.* **2020**, *317*, 128217. [[CrossRef](#)]
32. Zheng, Y.; Li, M.; Wen, X.; Ho, H.P.; Lu, H. Nanostructured ZnO/Ag film prepared by magnetron sputtering method for fast response of ammonia gas detection. *Molecules* **2020**, *25*, 1899. [[CrossRef](#)]
33. Tu, Y.; Kyle, C.; Luo, H.; Zhang, D.W.; Das, A.; Briscoe, J.; Dunn, S.; Titirici, M.M.; Krause, S. Ammonia gas sensor response of a vertical zinc oxide nanorod-gold junction diode at room temperature. *ACS Sens.* **2020**, *5*, 3568–3575. [[CrossRef](#)]
34. Wang, Z.; Zhu, L.; Sun, S.; Wang, J.; Yan, W. One-dimensional nanomaterials in resistive gas sensor: From material design to application. *Chemosensors* **2021**, *9*, 198. [[CrossRef](#)]
35. Zhang, J.; Liu, X.; Neri, G.; Pinna, N. Nanostructured materials for room-temperature gas sensors. *Adv. Mater.* **2016**, *28*, 795–831. [[CrossRef](#)]
36. Lun, D.; Xu, K. Recent progress in gas sensor based on nanomaterials. *Micromachines* **2022**, *13*, 919. [[CrossRef](#)]
37. Duan, X.; Duan, Z.; Zhang, Y.; Liu, B.; Li, X.; Zhao, Q.; Yuan, Z.; Jiang, Y.; Tai, H. Enhanced NH₃ sensing performance of polyaniline via a facile morphology modification strategy. *Sens. Actuators B Chem.* **2022**, *369*, 132302. [[CrossRef](#)]
38. Jamnani, S.R.; Moghaddam, H.M.; Leonardi, S.G.; Neri, G.; Ferlazzo, A. VOCs sensing properties of samarium oxide nanorods. *Ceram. Int.* **2024**, *50*, 403–411. [[CrossRef](#)]
39. Liang, Z.; Wang, M.; Liu, S.; Hassan, M.; Zhang, X.; Lei, S.; Qiao, G.; Liu, G. One-pot hydrothermal synthesis of self-assembled MoS₂/WS₂ nanoflowers for chemiresistive room-temperature NO₂ sensors. *Sens. Actuators B Chem.* **2024**, *403*, 135215. [[CrossRef](#)]
40. Duan, X.; Jiang, Y.; Liu, B.; Duan, Z.; Zhang, Y.; Yuan, Z.; Tai, H. Enhancing the carbon dioxide sensing performance of LaFeO₃ by Co doping. *Sens. Actuators B Chem.* **2024**, *402*, 135136. [[CrossRef](#)]
41. Li, J.; Ma, Y.; Duan, Z.; Zhang, Y.; Duan, X.; Liu, B.; Yuan, Z.; Wu, Y.; Jiang, Y.; Tai, H. Local dynamic neural network for quantitative analysis of mixed gases. *Sens. Actuators B Chem.* **2024**, *404*, 135230. [[CrossRef](#)]
42. Guo, Y.; Liu, B.; Duan, Z.; Yuan, Z.; Jiang, Y.; Tai, H. Batch fabrication of H₂S sensors based on evaporated Pd/WO₃ film with ppb-level detection limit. *Mater. Chem. Phys.* **2023**, *302*, 127768. [[CrossRef](#)]
43. Yuan, Z.; Zhao, Q.; Duan, Z.; Xie, C.; Duan, X.; Li, S.; Ye, Z.; Jiang, Y.; Tai, H. Ag₂Te nanowires for humidity-resistant trace-level NO₂ detection at room temperature. *Sens. Actuators B Chem.* **2022**, *363*, 131790. [[CrossRef](#)]
44. Zhang, Y.; Duan, Z.; Zou, H.; Ma, M. Fabrication of electrospun LaFeO₃ nanotubes via annealing technique for fast ethanol detection. *Mater. Lett.* **2018**, *215*, 58–61. [[CrossRef](#)]
45. Zhao, Q.; Duan, Z.; Yuan, Z.; Li, X.; Si, W.; Liu, B.; Zhang, Y.; Jiang, Y.; Tai, H. High performance ethylene sensor based on palladium-loaded tin oxide: Application in fruit quality detection. *Chin. Chem. Lett.* **2020**, *31*, 2045–2049. [[CrossRef](#)]
46. Ferlazzo, A.; Espro, C.; Iannazzo, D.; Moulaei, K.; Neri, G. A novel yttria-doped ZrO₂ based conductometric sensor for hydrogen leak monitoring. *Int. J. Hydrog. Energy* **2022**, *47*, 9819–9828. [[CrossRef](#)]
47. Yousefi, R.; Zak, A.K.; Mahmoudian, M.R. Growth and characterization of Cl-doped ZnO hexagonal nanodisks. *J. Solid State Chem.* **2011**, *184*, 2678–2682. [[CrossRef](#)]
48. Wang, M.; Hahn, S.H.; Kim, J.S.; Chung, J.S.; Kim, E.J.; Koo, K.K. Solvent-controlled crystallization of zinc oxide nano(micro)disks. *J. Cryst. Growth* **2008**, *310*, 1213–1219. [[CrossRef](#)]
49. Ramzan Parra, M.; Pandey, P.; Siddiqui, H.; Sudhakar, V.; Krishnamoorthy, K.; Haque, F.Z. Evolution of ZnO nanostructures as hexagonal disk: Implementation as photoanode material and efficiency enhancement in Al: ZnO based dye sensitized solar cells. *Appl. Surf. Sci.* **2019**, *470*, 1130–1138. [[CrossRef](#)]
50. Zhao, Q.; Shen, Q.; Yang, F.; Zhao, H.; Liu, B.; Liang, Q.; Wei, A.; Yang, H.; Liu, S. Direct growth of ZnO nanodisk networks with an exposed (0001) facet on Au comb-shaped interdigitating electrodes and the enhanced gas-sensing property of polar {0001} surfaces. *Sens. Actuators B Chem.* **2014**, *195*, 71–79. [[CrossRef](#)]
51. Gao, J.; Wu, B.; Cao, C.; Zhan, Z.; Ma, W.; Wang, X. Unraveling the dynamic evolution of Pd species on Pd-loaded ZnO nanorods for different hydrogen sensing behaviors. *ACS Sustain. Chem. Eng.* **2021**, *9*, 6370–6379. [[CrossRef](#)]
52. Ganesh, R.S.; Durgadevi, E.; Navaneethan, M.; Patil, V.L.; Ponnusamy, S.; Muthamizhchelvan, C.; Kawasaki, S.; Patil, P.S.; Hayakawa, Y. Controlled synthesis of Ni-doped ZnO hexagonal microdiscs and their gas sensing properties at low temperature. *Chem. Phys. Lett.* **2017**, *689*, 92–99. [[CrossRef](#)]
53. Liu, J.; Zhang, L.; Fan, J.; Zhu, B.; Yu, J. Triethylamine gas sensor based on Pt-functionalized hierarchical ZnO microspheres. *Sens. Actuators B Chem.* **2021**, *331*, 129425. [[CrossRef](#)]
54. Zhang, Y.; Jiang, Y.; Yuan, Z.; Liu, B.; Zhao, Q.; Huang, Q.; Li, Z.; Zeng, W.; Duan, Z.; Tai, H. Synergistic effect of electron scattering and space charge transfer enabled unprecedented room temperature NO₂ sensing response of SnO₂. *Small* **2023**, *19*, 2303631. [[CrossRef](#)]
55. Li, C.F.; Hsu, C.Y.; Li, Y.Y. NH₃ sensing properties of ZnO thin films prepared via sol-gel method. *J. Alloys Compd.* **2014**, *606*, 27–31. [[CrossRef](#)]

56. Majumder, D.; Roy, S. Room temperature synthesis of TiO₂ nanospheres: Ammonia sensing characteristics. *Mater. Today Proc.* **2018**, *5*, 9811–9816. [[CrossRef](#)]
57. Pan, F.; Lin, H.; Zhai, H.; Miao, Z.; Zhang, Y.; Xu, K.; Guan, B.; Huang, H.; Zhang, H. Pd-doped TiO₂ film sensors prepared by premixed stagnation flames for CO and NH₃ gas sensing. *Sens. Actuators B Chem.* **2018**, *261*, 451–459. [[CrossRef](#)]
58. Lavanya, N.; Anithaa, A.C.; Sekar, C.; Asokan, K.; Bonavita, A.; Donato, N.; Leonardi, S.G.; Neri, G. Effect of gamma irradiation on structural, electrical and gas sensing properties of tungsten oxide nanoparticles. *J. Alloys Compd.* **2017**, *693*, 366–372. [[CrossRef](#)]
59. Samà, J.; Barth, S.; Domènech-Gil, G.; Prades, J.D.; López, N.; Casals, O.; Gràcia, I.; Cané, C.; Romano-Rodríguez, A. Site-selectively grown SnO₂ NWs networks on micromembranes for efficient ammonia sensing in humid conditions. *Sens. Actuators B Chem.* **2016**, *232*, 402–409. [[CrossRef](#)]
60. Gayathri, K.; Ravichandran, K.; Sridharan, M.; Suvathi, S.; Sriram, S.; Mohan, R.; Jansi Santhosam, A.; Praseetha, P.K.; Sakthivel, P. Enhanced ammonia gas sensing by cost-effective SnO₂ gas sensor: Influence of effective Mo doping. *Mater. Sci. Eng. B* **2023**, *298*, 116849. [[CrossRef](#)]
61. Tong, Y.; Zhang, Y.; Jiang, B.; He, J.; Zheng, X.; Liang, Q. Effect of lanthanides on acetone sensing properties of LnFeO₃ nanofibers (Ln = La, Nd, and Sm). *IEEE Sens. J.* **2017**, *17*, 2404–2410. [[CrossRef](#)]

Disclaimer/Publisher’s Note: The statements, opinions and data contained in all publications are solely those of the individual author(s) and contributor(s) and not of MDPI and/or the editor(s). MDPI and/or the editor(s) disclaim responsibility for any injury to people or property resulting from any ideas, methods, instructions or products referred to in the content.